Investigation of Particle Coherence in Pb+Pb Collisions at LHC

Bengt Henrik Brusheim Johansson

The evolution of matter

The "known" matter has evolved for $\sim 10^5$ years until observable. The conditions are believed to have been extreme.

The "Primordial Matter" transits through hot and dense exotic phases on its way to observable hadrons.

High energy experiments are believed to reproduce these conditions, thus providing for "observation" of hadronization processes.

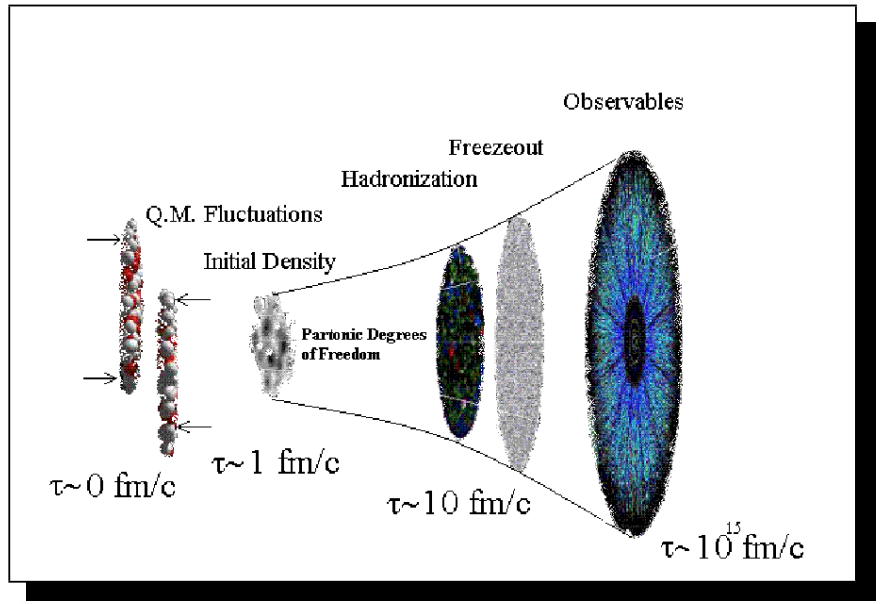

Figure 1: Hadronization

Evolution of participant matter

The collision participants form the initial conditions for an evolution characterized by pressure gradients and *in medio* modulations, thus producing a momentum anisotropy.

This anisotropy, "flow", is in general contextualized as Fourier terms (1) in the particle yield expansion observed in the detector.

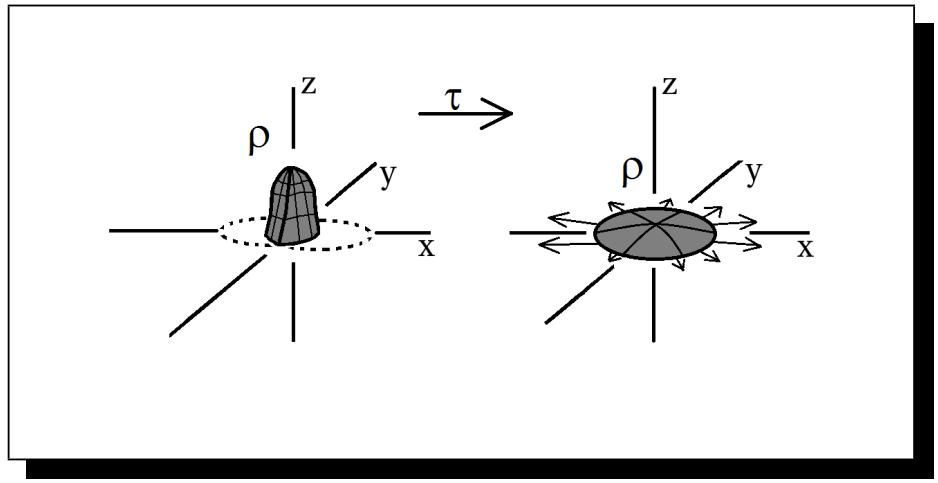

Figure 2: Evolution of matter

Flow is thus an observable connected to initial conditions and strong interactions; including phase transitions.

$$E\frac{d^3N}{d^3p} = E\frac{d^2N}{2\pi p_T dp_T d\eta} \times \{1 + 2\sum_{n=1}^{\infty} v_n(p_T,\eta)\cos[n(\phi - \Psi_n)]\} \quad (1)$$

The Model Implementation

The model [1] implements the second and third event plane. The fireball deformation is simulated in terms of event planes. The transverse radius is modelled as

$$R(b,\phi,\epsilon) = R_f(b)\frac{\sqrt{1-\epsilon(b)^2}}{\sqrt{1+\epsilon(b)\cos(2\phi)}}\ . \tag{2}$$

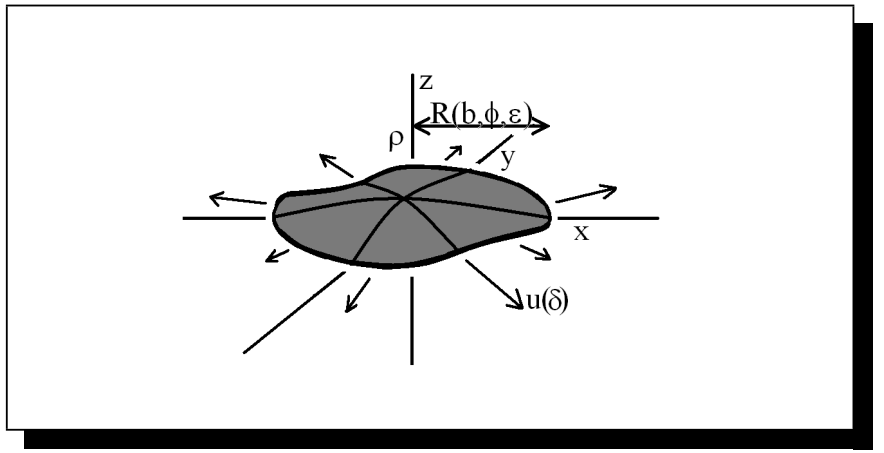

Figure 3: Model Parameters

Further, the linear transverse rapidity profile $\tilde{\rho_u}$ is modelled as

$$\tilde{\rho_u} = \frac{r}{R_f(b)}\rho_u^{max} f(\Psi_3,\ldots). \tag{3}$$

Flow is simulated with two model flow parameters: δ modulates the velocities; and ϵ modulates the azimuth in the expressions above.

Generating the State

Present model is a superposition of parameterized hydrodynamics and generated hard states [1]. The events, characterized by the impact parameter; are generated in the multiple scattering Glauber model, with in-elastic cross section

$$\frac{d^2\sigma_{in}^{AA}}{d^2b} = \left[1 - \left(1 - \frac{T_{AA}(b)\sigma_{NN}^{in}(\sqrt{s})}{A^2}\right)^{A^2}\right]. \tag{4}$$

The hard and soft yields are simulated as

$$\bar{N}_{bin}\left(b, \sqrt{s}\right) = T_{AA}\sigma_{NN}^{inel.} \tag{5}$$

$$\bar{N}_{part}\left(b, \sqrt{s}\right) = \int d^2\mathbf{x} T_A(r_1)\left[1 - \exp(\sigma_{NN}^{inel.} T_A(r_2))\right]. \tag{6}$$

The soft and hard state are simulated simultaneously and form together the yield.

Generation of the Soft State

The "thermal" soft state is generated on the freeze out hyper-surfaces of the expanding particle distribution, with preset freeze-out temperatures and chemical potentials.

The particle density flux is integrated over the freeze-out hypersurface, thus producing a mean specie multiplicity ($\bar{N}_i$). The model particle number probability is given by the Poisson distribution

$$P(N_i) = \exp(-\bar{N}_i)\frac{\bar{N}_i^N}{N_i!} \ . \tag{7}$$

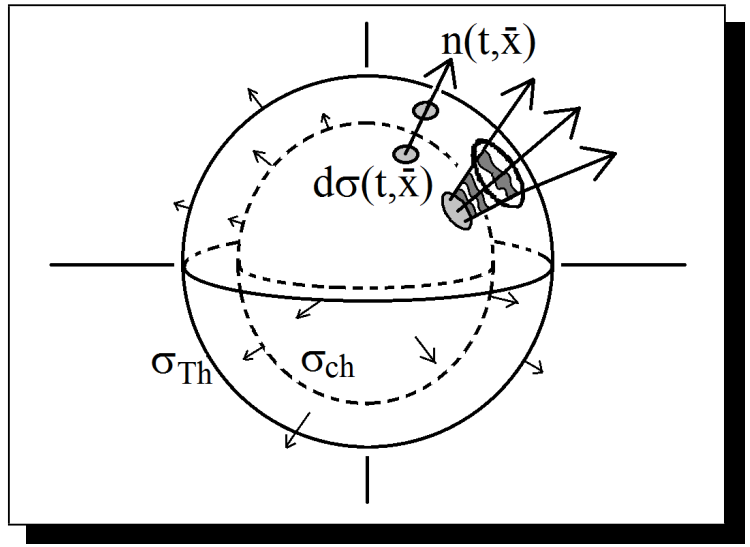

Figure 4: Freeze-out Hyper Surfaces

Freeze-out is only determined by the parameterized temperature and chemical baryon potential

$$T(\mu_B) = a - b\mu_B^2 - c\mu_B^4, \quad \mu_B = \frac{d}{1+e\sqrt{s_{NN}}}. \tag{8}$$

Generation of the Hard State

The number of sub collisions are generated thus providing a collection subject to hard processes.

The type of hard collisions are determined with simple selection criteria.

Generation of jet vertex is based on participant density.

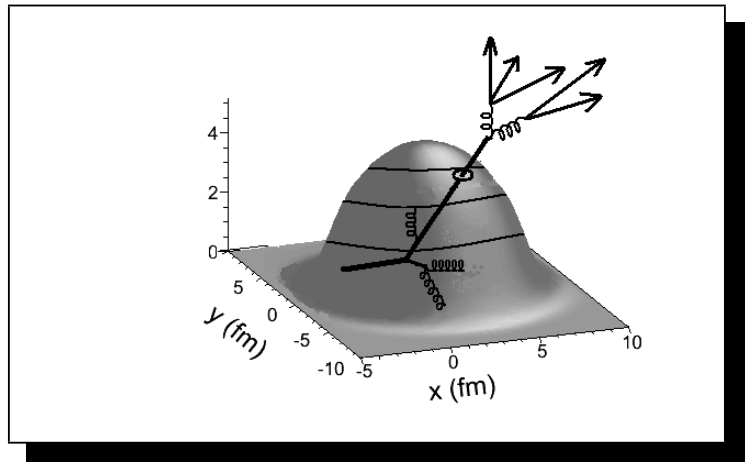

Figure 5: Hard Scattering, including jet vertex

$$\frac{dN^{jet}}{d\Psi r dr} = \frac{T_A(r_1)T_A(r_2)}{T_{AA}(b)}. \quad (9)$$

Jet quenching is simulated on "hard" particles as of below.

Particle Decays

Particle decays are run with particle data and branching ratios from the SHARE table [2], which contains 360 particles. The resonance mass distribution is given by the Breit-Wigner distribution

$$\boxed{P(m)dm \propto \frac{1}{(m-m_0)^2+\Delta m^2/4}\cdot} \tag{10}$$

with the decay probability given by

$$\boxed{P(\tau) \propto \Gamma \exp(\Gamma\tau),} \tag{11}$$

where $1/\Gamma$ is the resonance life-time.

Medium Dynamics

Medium expansion is modelled as a longitudinal expanding quark-gluon fluid. Conservation of the energy momentum tensor provides the Bjorken scaling laws for the medium.

The conservation laws provides (proper) time dependecies for the energy density $\epsilon(\tau)$, temperature $T(\tau)$ and density $\rho(\tau)$

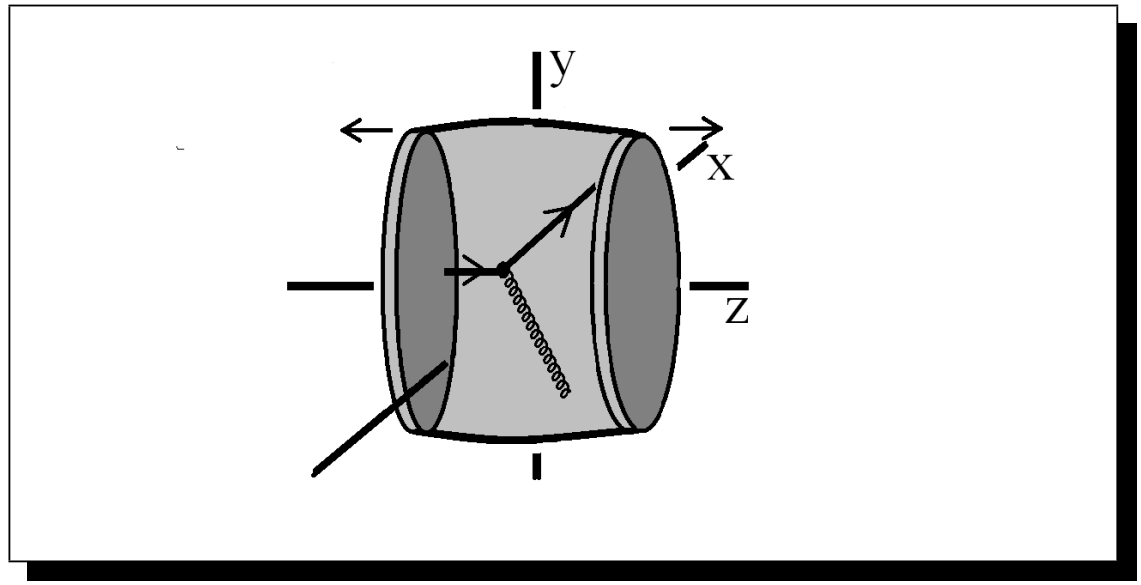

Figure 6: Medium Expansion

$$\epsilon(\tau)\tau^{4/3} = \epsilon_0\tau_0^{4/3}, \quad T(\tau)\tau^{1/3} = T_0\tau_0^{1/3}, \quad \rho(\tau)\tau = \rho_0\tau_0 \ . \tag{12}$$

In Medio Evolution

The *in medio* radiative modulation of the parton energy is treated in the BDMS framework.

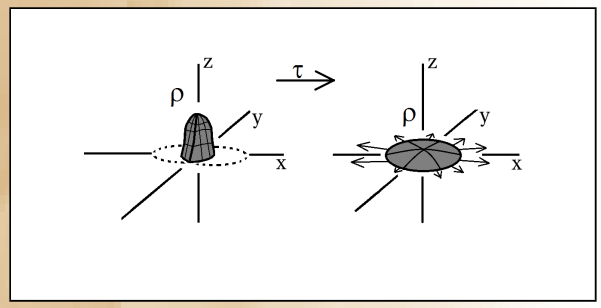

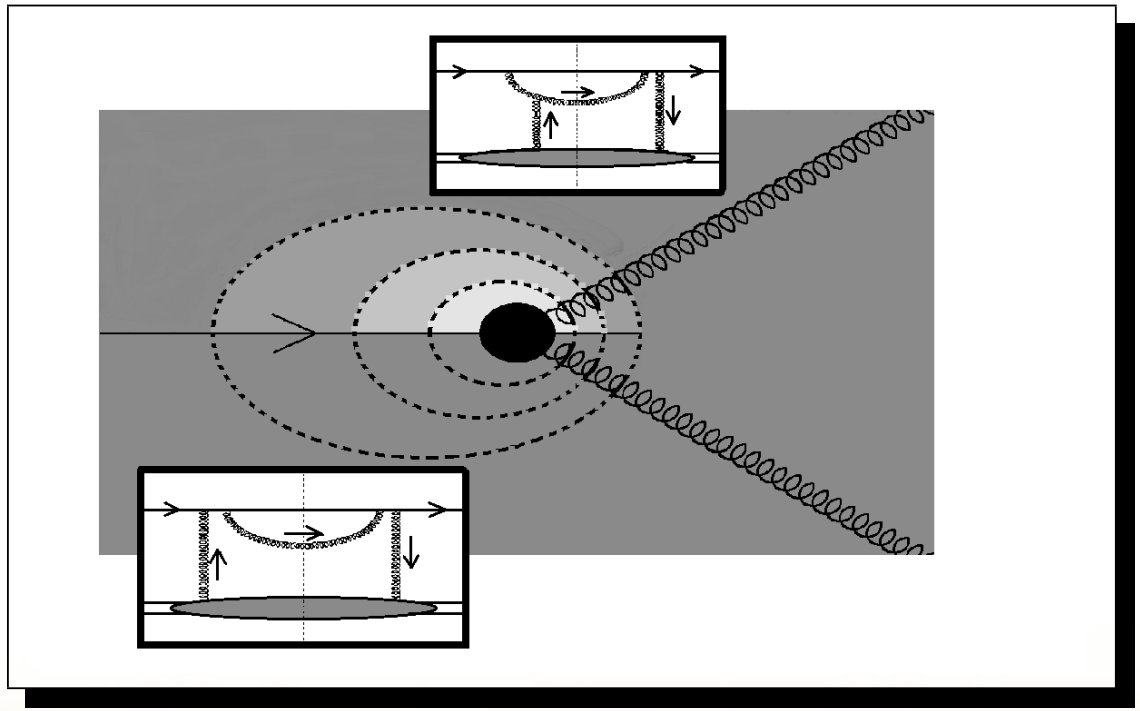

Figure 7: Main modes of energy loss in BDMS framework.

Collisional energy loss

The energy loss due to in-media collisions in the high momentum transfer limit is

$$\Delta E = \frac{1}{4T\rho}\int_0^L dl \int_{\mu_D^2}^{t_{max}} dt \frac{d\sigma}{dt} t \tag{13}$$

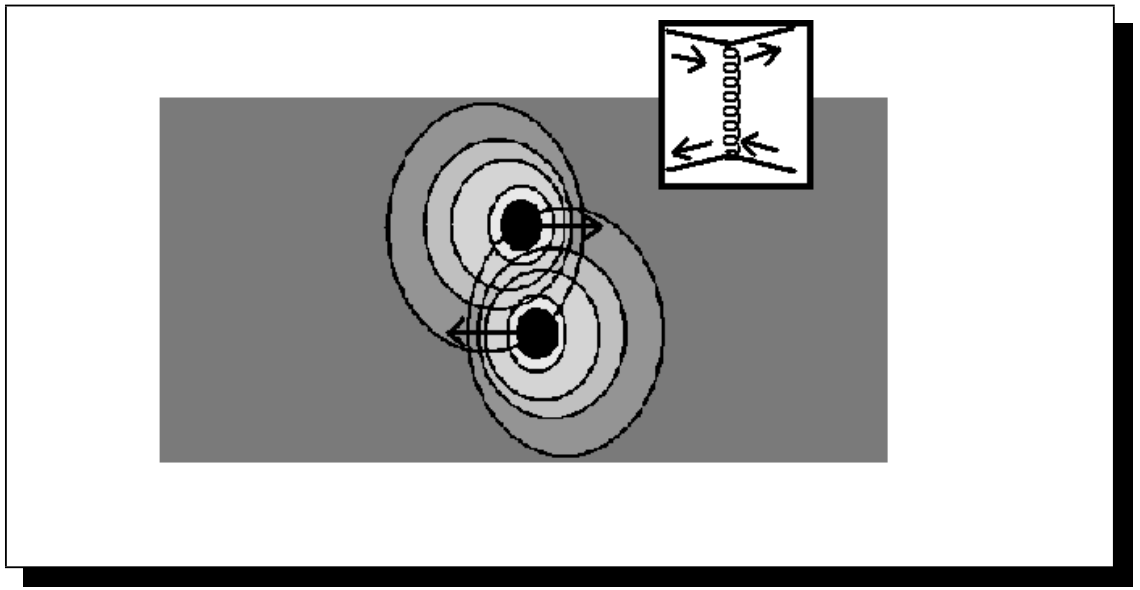

Characteristics of Heavy Ion Collisions

... modern high energy experiments reproduces the hot and dense conditions of the early universe.

Characteristics of Heavy Ion Collisions

... modern high energy experiments reproduces the hot and dense conditions of the early universe.

... momentum anisotropy is a consequence of pressure gradients in the initial density distribution.

Characteristics of Heavy Ion Collisions

... modern high energy experiments reproduces the hot and dense conditions of the early universe.

... momentum anisotropy is a consequence of pressure gradients in the initial density distribution.

... a detailed partially parameterized model, HYDJET++, describes the *in medio* modulations, which are defining for the observable distributions.

Characteristics of Heavy Ion Collisions

... modern high energy experiments reproduces the hot and dense conditions of the early universe.

... momentum anisotropy is a consequence of pressure gradients in the initial density distribution.

... a detailed partially parameterized model, HYDJET++, describes the *in medio* modulations, which are defining for the observable distributions.

... In the model, the simulated yield is a superposition of soft and hard particles.

Simulating the particle spectra

The generated spectra agrees with experimental data. The simulation of the particle spectra provides a base for the investigation of RHIC's.

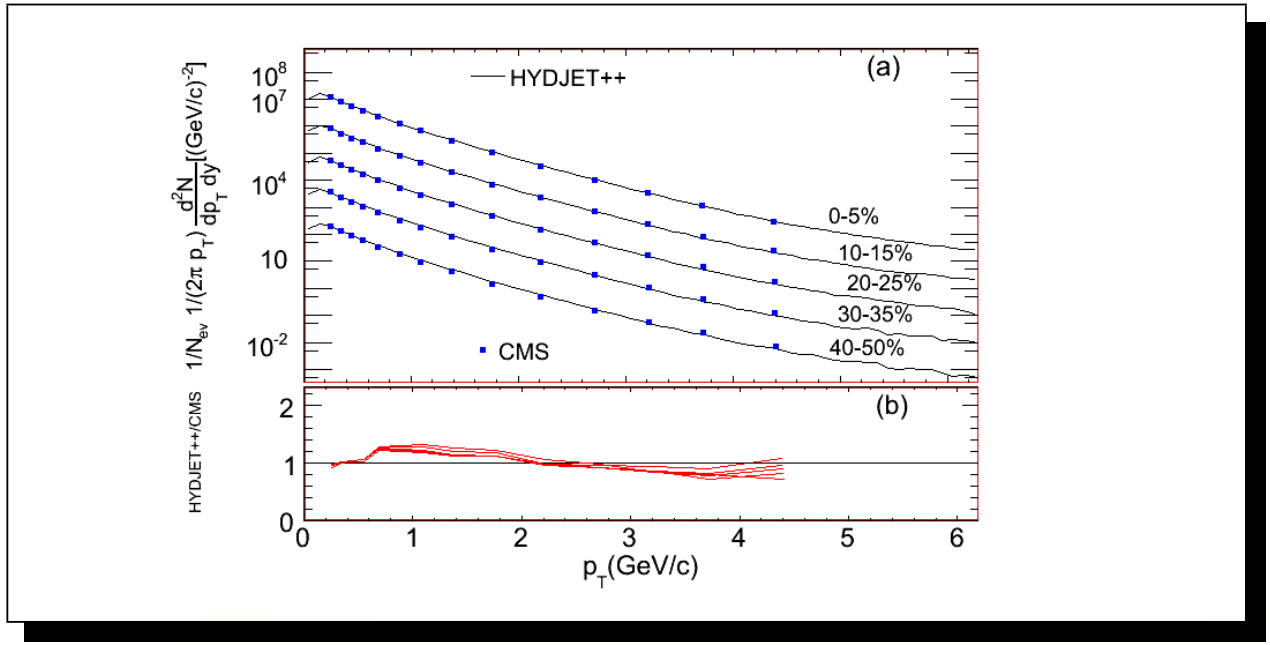

Figure 8: Particle spectra. Simulations are compared with experimental data. Simulations made for centralities: $\sigma/\sigma_0 = 0-5\%,\ 10-20\%,\ 20-30\%,\ 30-40\%,\ 40-50\%$

The thermal projection of the particle spectra

Hydrodynamical spectra are projected.

In the model, hydrodynamics is dominating the $0 < p_T < 1.5$ GeV/c regime of the particle spectra.

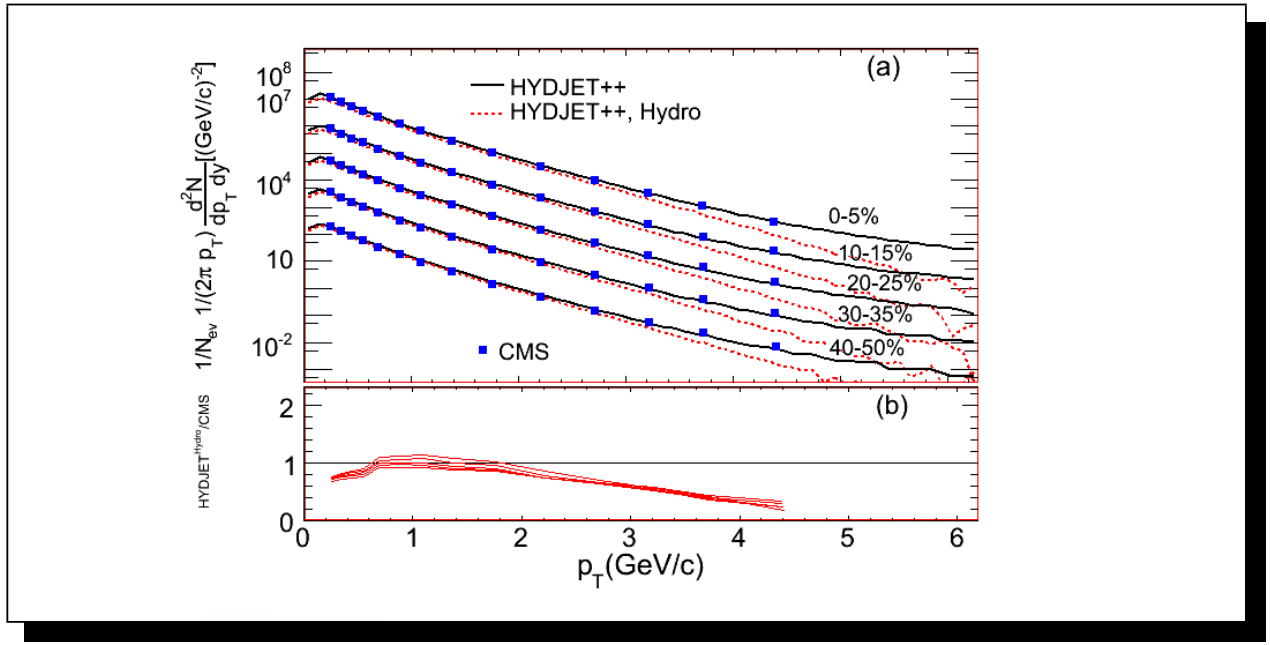

Figure 9: Particle spectra with hydrodynamical projection included.

Generating the elliptic flow

The azimuthal anisotropy is simulated. The simulation is done for $\sqrt{s} = 2.76$ TeV and $|\eta| < 2.5$, and compared with experimental data [3].

Here, the elliptic flow is displayed, including the hydrodynamical projection.

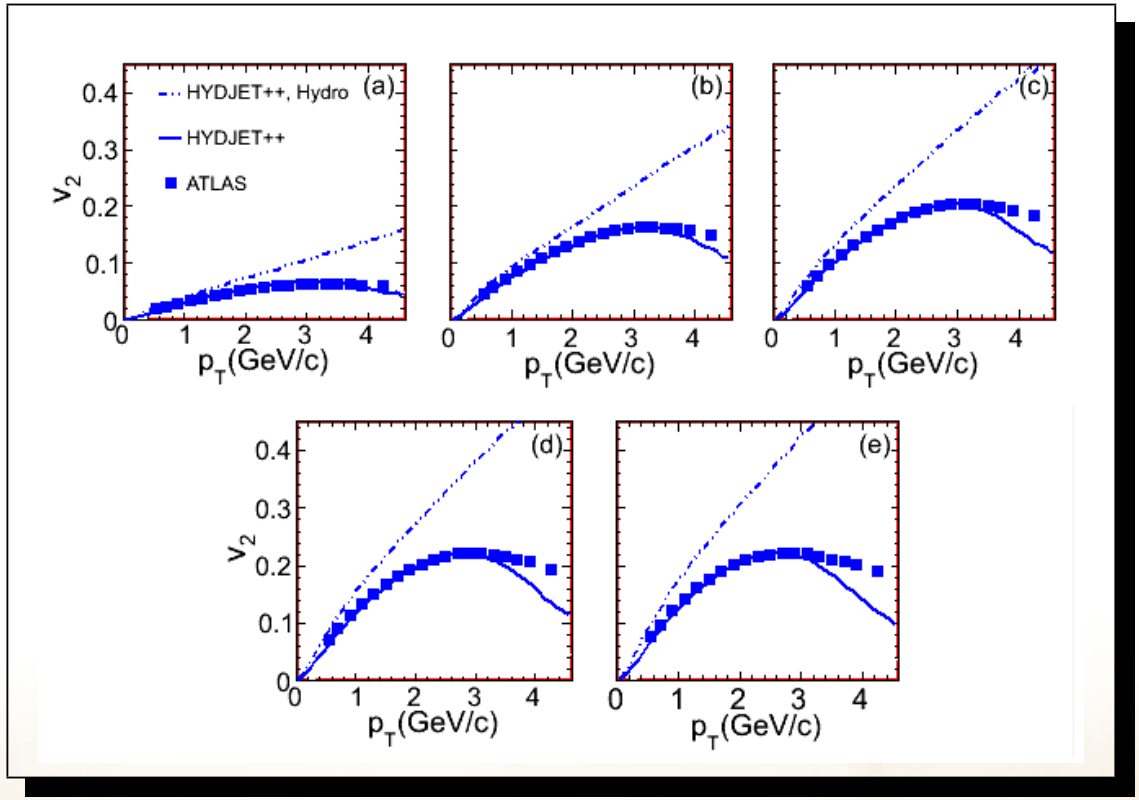

Figure 10: Elliptic Flow. The elliptic flow is simulated for the centralities: $\sigma/\sigma_0 = 0 - 5\%$, $10 - 20\%$, $20 - 30\%$, $30 - 40\%$, $40 - 50\%$.

Projecting the triangular flow

Triangular flow is also simulated in the HYDJET++ model.

The fluctuation dependent flow is extracted, thus displaying a first order simulation of the initial geometry, which is compared with experimental data [3].

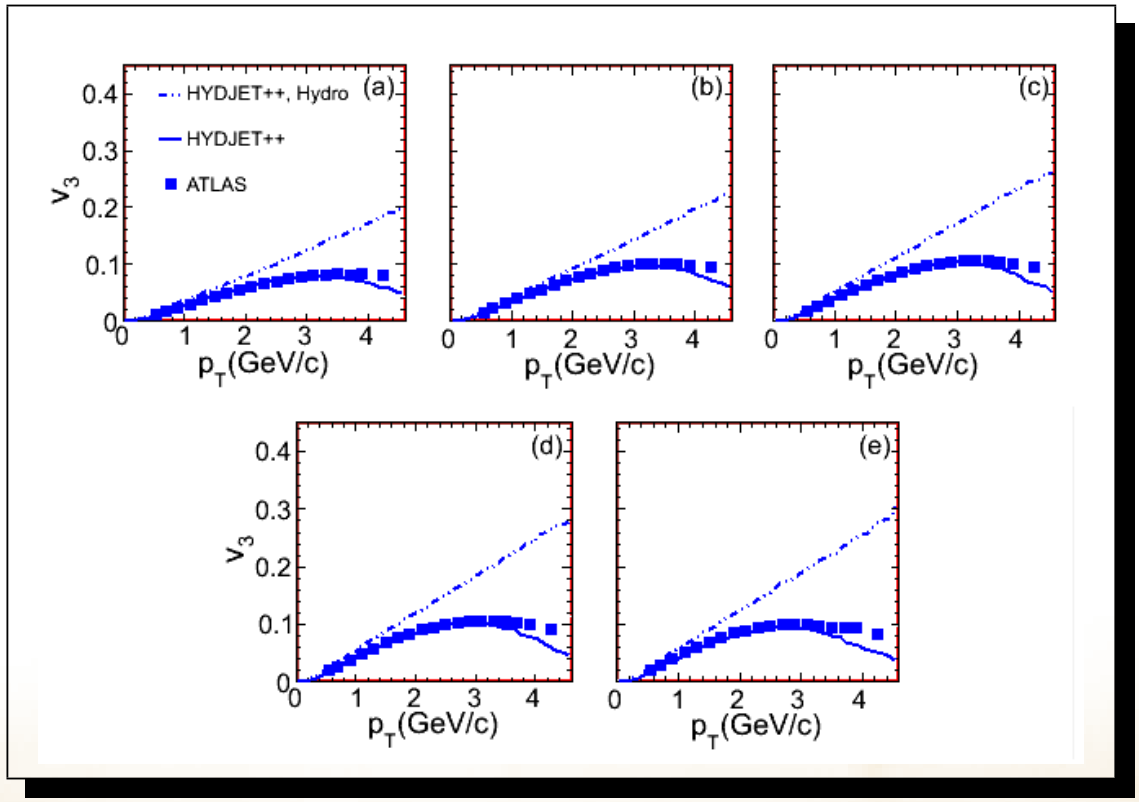

Figure 11: Triangular Flow. The triangular flow is simulated for the centralities: $\sigma/\sigma_0 = 0-5\%$, $10-20\%$, $20-30\%$, $30-40\%$, $40-50\%$.

Pentagonal flow

Pentagonal flow is simulated in the HYDJET++ model.

"Non-Linear" pentagonal flow is included. Eventplane mixing is observed.

Experimental ATLAS data are included [3].

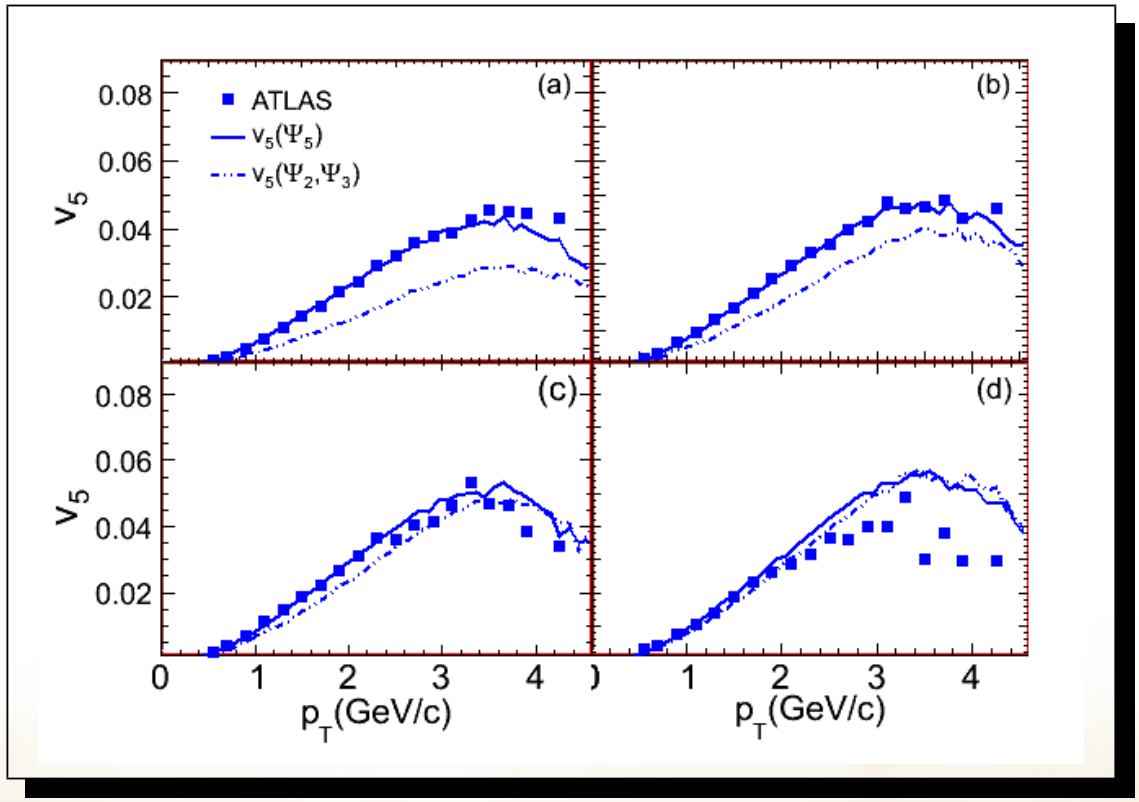

Figure 12: Pentagonal Flow. Flow is simulated for the centralities: $\sigma/\sigma_0 = 10-20\%,\ 20-30\%,\ 30-40\%,\ 40-50\%$.

Quadrangular flow

Quadrangular flow is simulated in the HYDJET++ model.

Hydrodynamical projection is included. Simulation only made in Ψ_2 plane and compared to ALICE (Ψ_2) data [4].

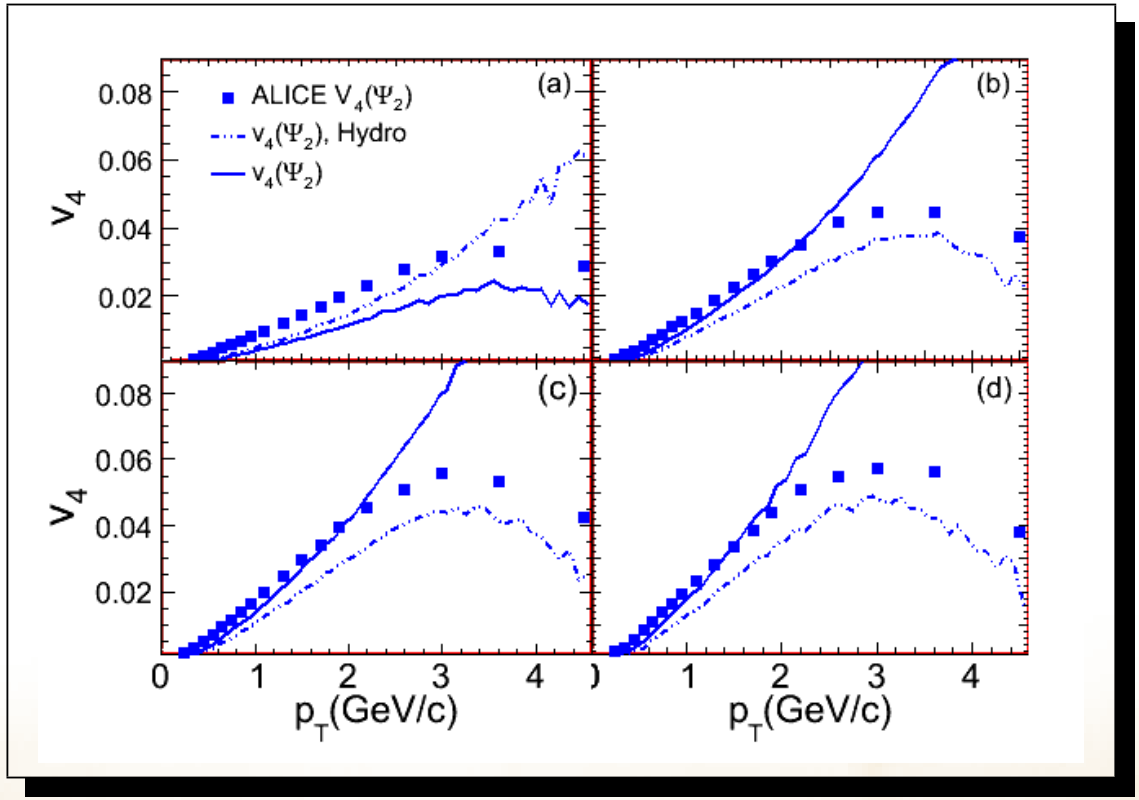

Figure 13: Quadrangular Flow. Flow is simulated for the centralities: $\sigma/\sigma_0 = 10-20\%$, $20-30\%$, $30-40\%$, $40-50\%$.

Centrality dependence of the elliptic and triangular flow

The flow is integrated in the HYDJET++ model. Comparison with experimental data [3].

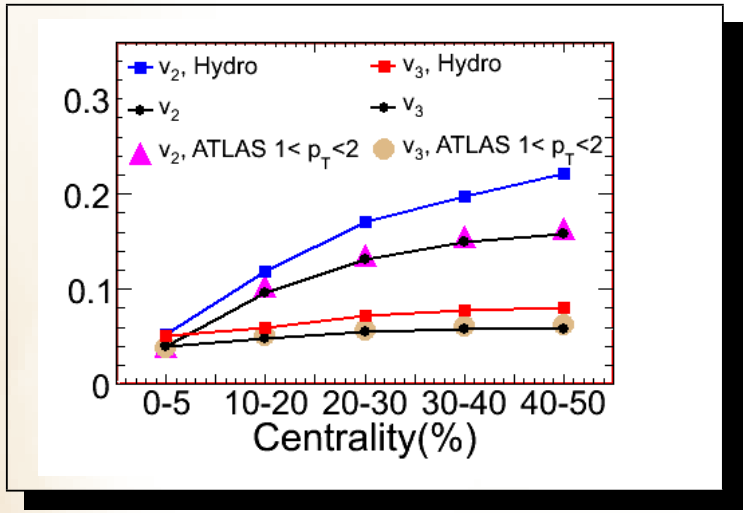

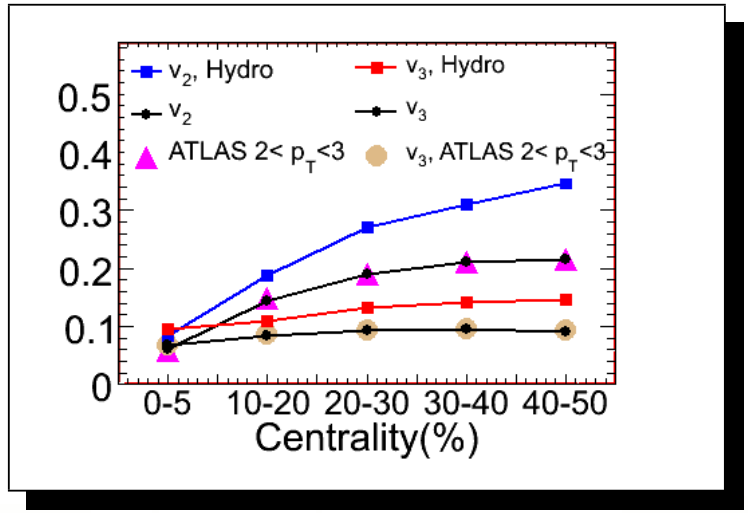

Recaption

... modern high energy experiments reproduces the hot and dense conditions of the early universe.

... momentum anisotropy is a consequence of pressure gradients in the initial density distribution.

... a detailed partially parameterized model describes the *in medio* modulations, which are defining for the observable distributions.

... the generated spectra, including hydrodynamical projection corresponds to a fair degree with experimental data.

Recaption

... modern high energy experiments reproduces the hot and dense conditions of the early universe.

... momentum anisotropy is a consequence of pressure gradients in the initial density distribution.

... a detailed partially parameterized model describes the *in medio* modulations, which are defining for the observable distributions.

... the generated spectra, including hydrodynamical projection corresponds to a fair degree with experimental data.

... the elliptic, triangular; and pentagonal flow are reproduced.

Recaption

... modern high energy experiments reproduces the hot and dense conditions of the early universe.

... momentum anisotropy is a consequence of pressure gradients in the initial density distribution.

... a detailed partially parameterized model describes the *in medio* modulations, which are defining for the observable distributions.

... the generated spectra, including hydrodynamical projection corresponds to a fair degree with experimental data.

... the elliptic, triangular; and pentagonal flow are reproduced.

... Integrated flow agrees with experimental data to a high degree.

Recaption

... modern high energy experiments reproduces the hot and dense conditions of the early universe.

... momentum anisotropy is a consequence of pressure gradients in the initial density distribution.

... a detailed partially parameterized model describes the *in medio* modulations, which are defining for the observable distributions.

... the generated spectra, including hydrodynamical projection corresponds to a fair degree with experimental data.

... the elliptic, triangular; and pentagonal flow are reproduced.

... Integrated flow agrees with experimental data to a high degree.

... the quadrangular flow is simulated only in the Ψ_2 plane; thus displaying deviations.

Transverse momentum dependence of the ratio v_4/v_2^2

The ratio displays factorization breaking for higher transverse momentum. The ratio is made consits of $v_4(\Psi_2)$ data.

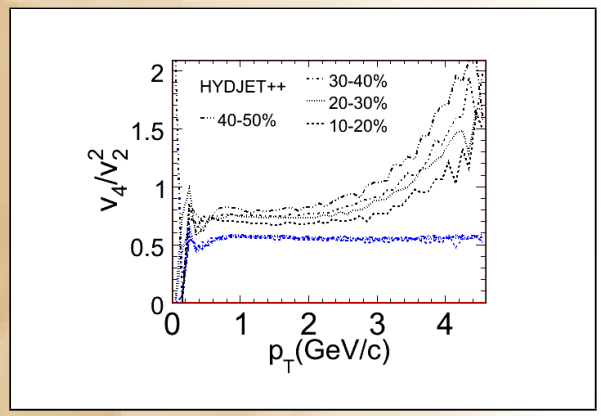

Hydrodynamical projection of the v_4/v_2^2 ratio is included (Blue). The factorization breaking in the inclusive flow is likely due to fluctuations, i.e. fragmentation processes.

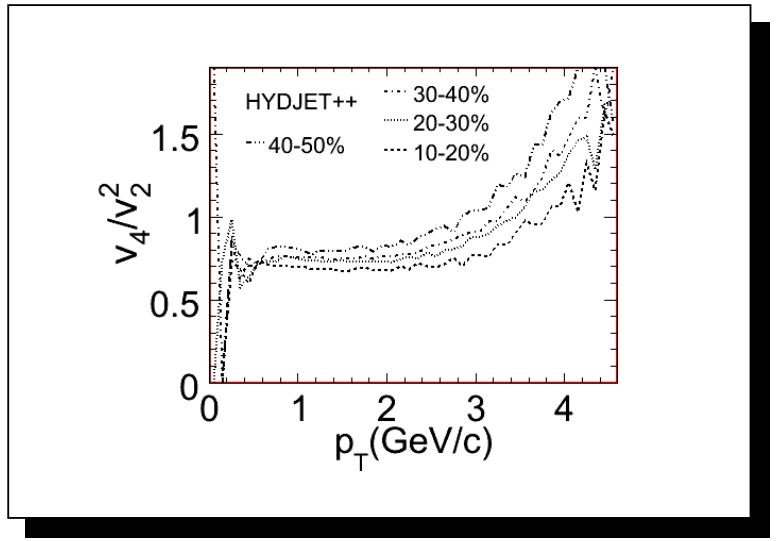

Figure 14: Ratio v_4/v_2^2.

Transverse momentum dependence of the ratio v_5/v_2v_3

The ratio displays scaling due to correlation between fifth order mixed-plane flow and elliptic and triangular flow.

The $v_5(\Psi_5)$ does not display the same type of scaling. The ratio depends on ellipticity due to non-correlating eventplanes.

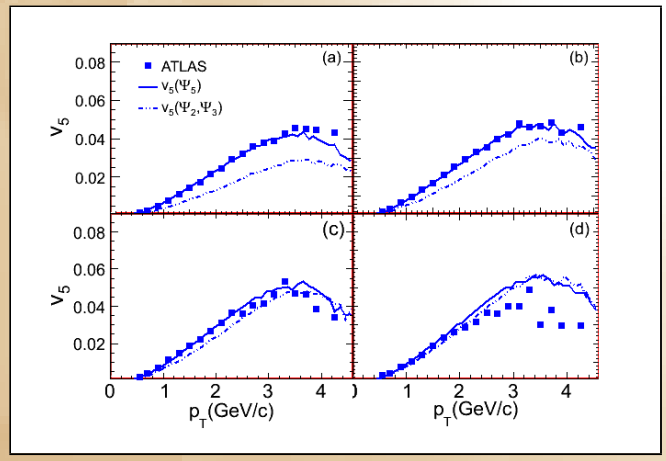

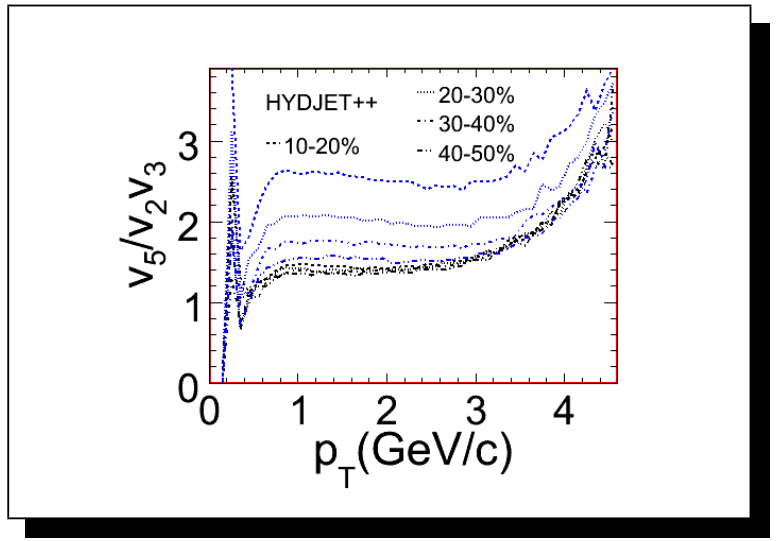

Figure 15: Ratio v_5/v_2v_3. Blue lines denote the ratio $v_5(\Psi_5)/v_2v_3$ and black lines denotes $v_5(\Psi_2,\Psi_3)/v_2v_3$.

Transverse momentum dependence of the ratio v_3^2/v_2^3

The ratio of the fluctuation dependent triangular flow (v_3), and ellipticity dependent elliptic flow (v_2), is investigated.

The ratio is seen to be Centrality (ellipticity) dependendent.

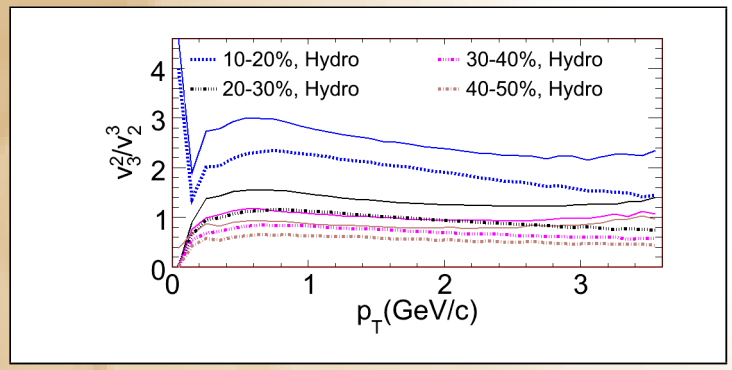

The hydrodynamic projection of the ratio is included. Factorization is seen to break due to less fluctuations (hydrodynamics).

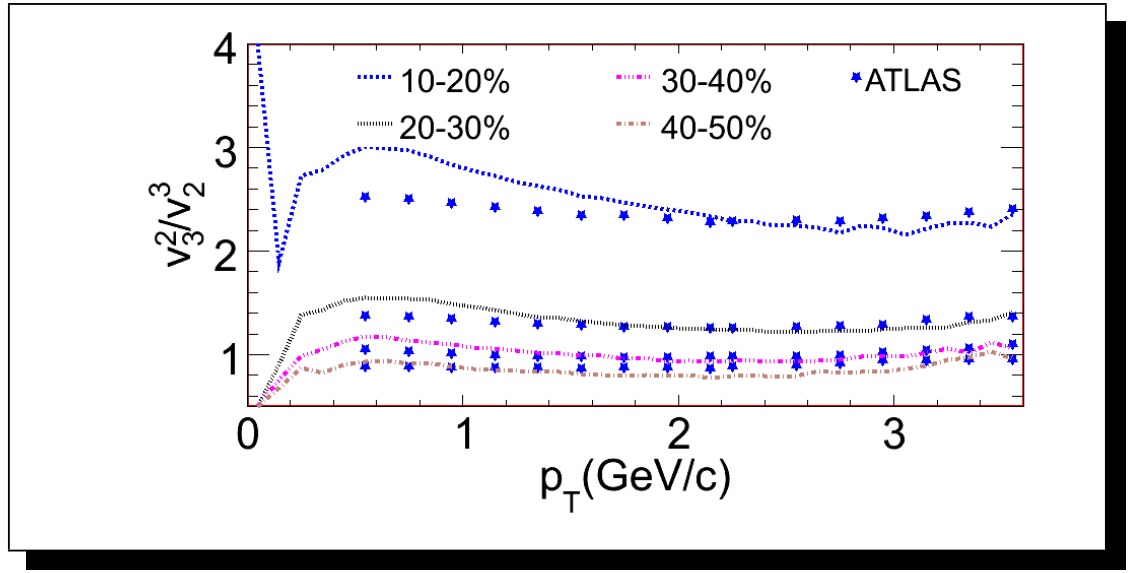

Figure 16: Ratio v_3^2/v_2^3

The ratio $v_6(\Psi_3)/v_6(\Psi_2)$

The sixth order flow corresponding to the factorization v_3^2/v_2^3 is simulated in the second and third eventplane.

Proportinality makes the ratio maintain the centrality hiearchy.

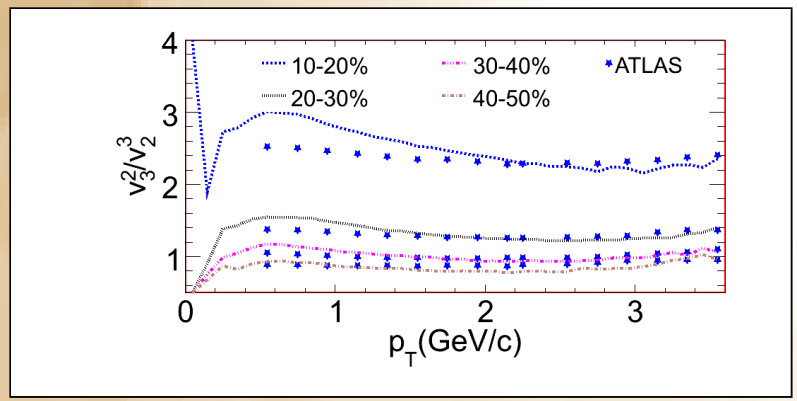

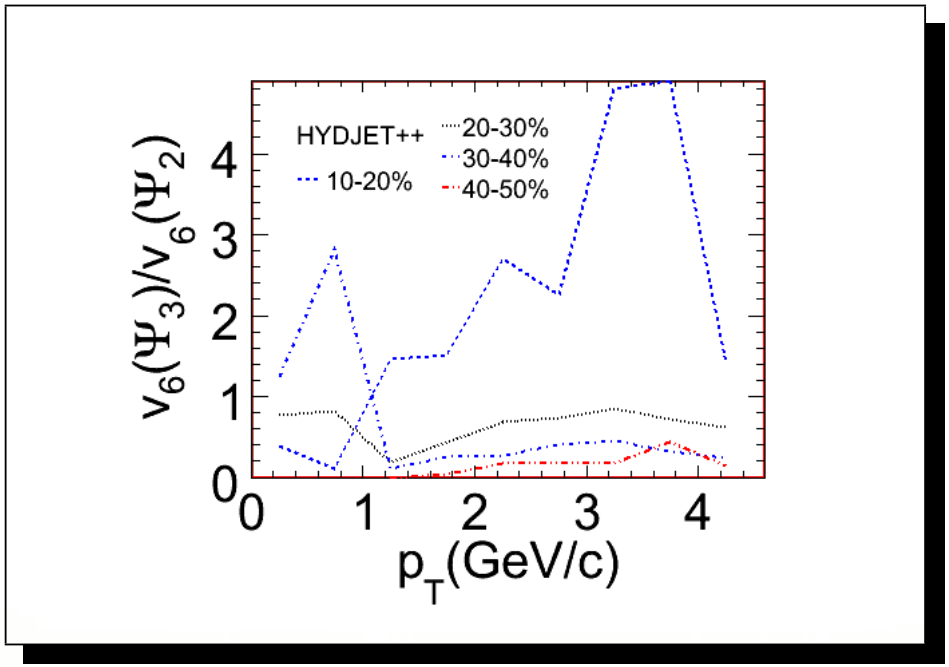

Figure 17: Ratio $v_6(\Psi_3)/v_6(\Psi_2)$

Integration of the ratio v_3^2/v_2^3

Integration of v_3/v_2 ratio.

Ratio is seen to depend on centrality in favour of elliptic flow.

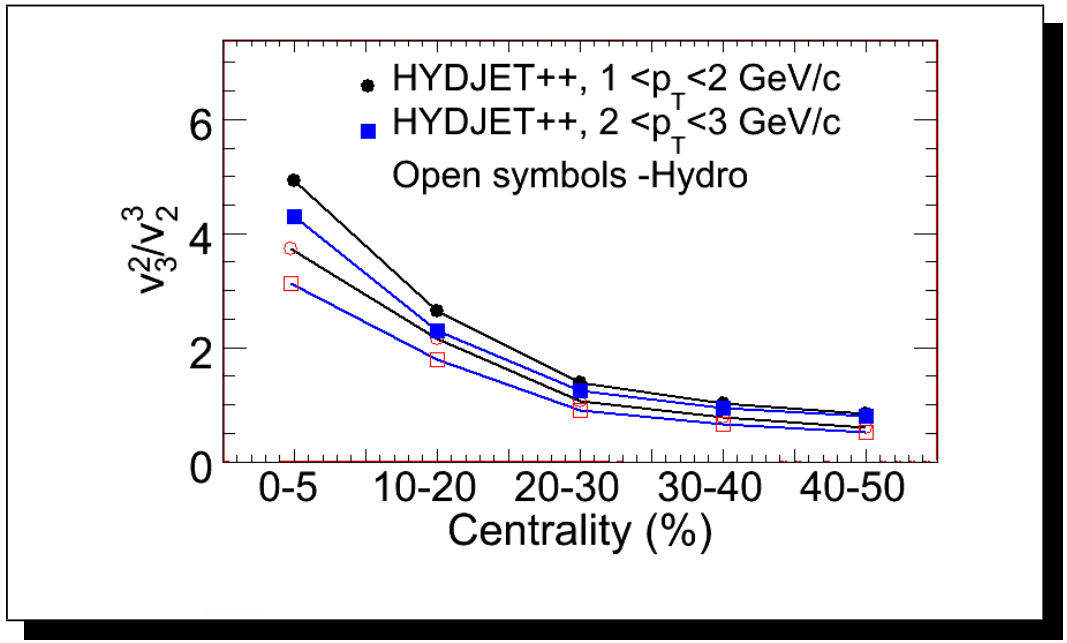

Figure 18: Particle spectra is simulated for the centralities: $\sigma/\sigma_0 = 0-5\%,\ 10-20\%,\ 20-30\%,\ 30-40\%,\ 40-50\%$.

Deviation from hydrodynamics for v_3^2/v_2^3 ratio.

...deviation from hydro is investigated as

$$\Delta = \frac{R - R^{Hydro}}{R}, \quad R = \frac{v_3^2}{v_2^3}$$

...quenching of ratio correlates with deviation from hydrodynamics.

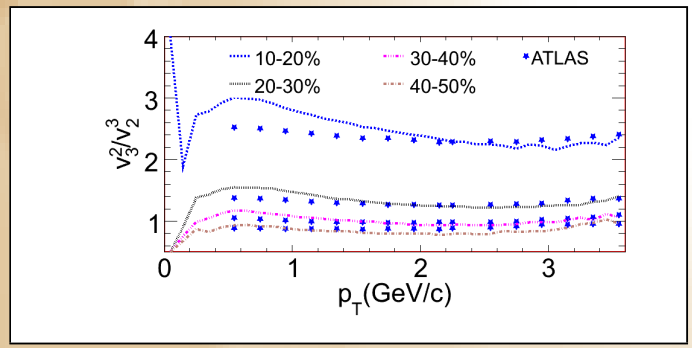

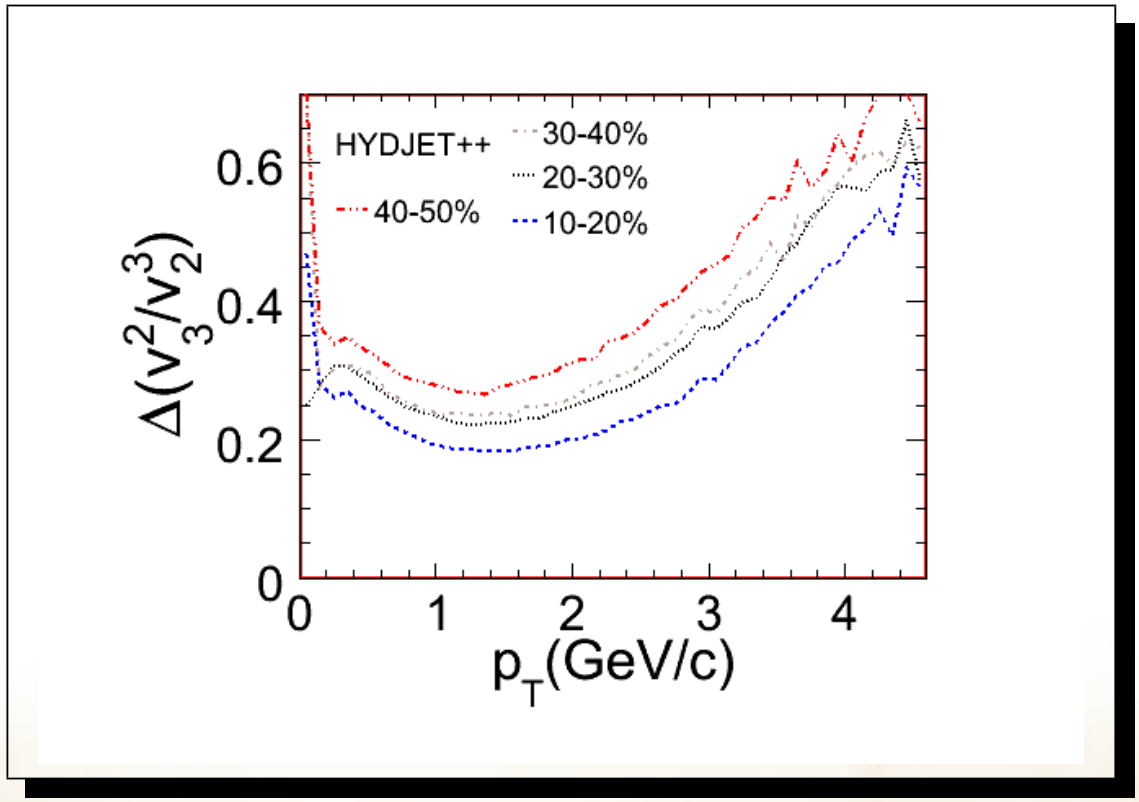

Figure 19: The relative deviation from hydrodynamics for the ratio v_3^2/v_2^3 is simulated for centralities.

On Results

Elliptic and triangular flow forms a base for further investigations. The characteristics of the flow projections are theoretically sound and agree with experimental data.

On Results

Elliptic and triangular flow forms a base for further investigations. The characteristics of the flow projections are theoretically sound and agree with experimental data.

Higher order flow displays characteristics which differs from lower order flow. The corresponding factorizations differentiates in terms of fluctuations. The different factorizations are seen to display features related to fluctuations and eventplane correlations.

On Results

Elliptic and triangular flow forms a base for further investigations. The characteristics of the flow projections are theoretically sound and agree with experimental data.

Higher order flow displays characteristics which differs from lower order flow. The corresponding factorizations differentiates in terms of fluctuations. The different factorizations are seen to display features related to fluctuations and eventplane correlations.

Eventplane mixing is visible in the displayed correlators, and makes for factorization.

In Conclusion

The elliptic and triangular flows are reproduced and form together with the reproducing of the transverse momentum spectra the foundation of further flow analysis.

In Conclusion

The elliptic and triangular flows are reproduced and form together with the reproducing of the transverse momentum spectra the foundation of further flow analysis.

The pentagonal flow is also seen to be reproduced to some extent. This enables a simulation of mixed eventplane flow. The mixed eventplane may provide for factorization.

In Conclusion

The elliptic and triangular flows are reproduced and form together with the reproducing of the transverse momentum spectra the foundation of further flow analysis.

The pentagonal flow is also seen to be reproduced to some extent. This enables a simulation of mixed eventplane flow. The mixed eventplane may provide for factorization.

The flow correlators i.e. higher order flow displays levels of factorization. Factorization is in general depending on fluctuations and eventplane correlations.

References

[1] I. P. Lokhtin, L. V. Malinina, S. V. Petrushanko, A. M. Snigirev, I. Arsene and K. Tywoniuk, **180**, 779 (2009)

[2] G. Torieri, S. Steinke, W. Broniowski, W. Florkowski, J. Letessier and J. Rafelski, Comp. Phys. Comm. **167**, 229 (2005).

[3] G. Aad *et al.* (ATLAS Collaboration), Phys. Rev. C **86**, 014907 (2012).

[4] B. Abelev *et al.* (ALICE Collaboration), arXiv:1205:5761v2

Summary

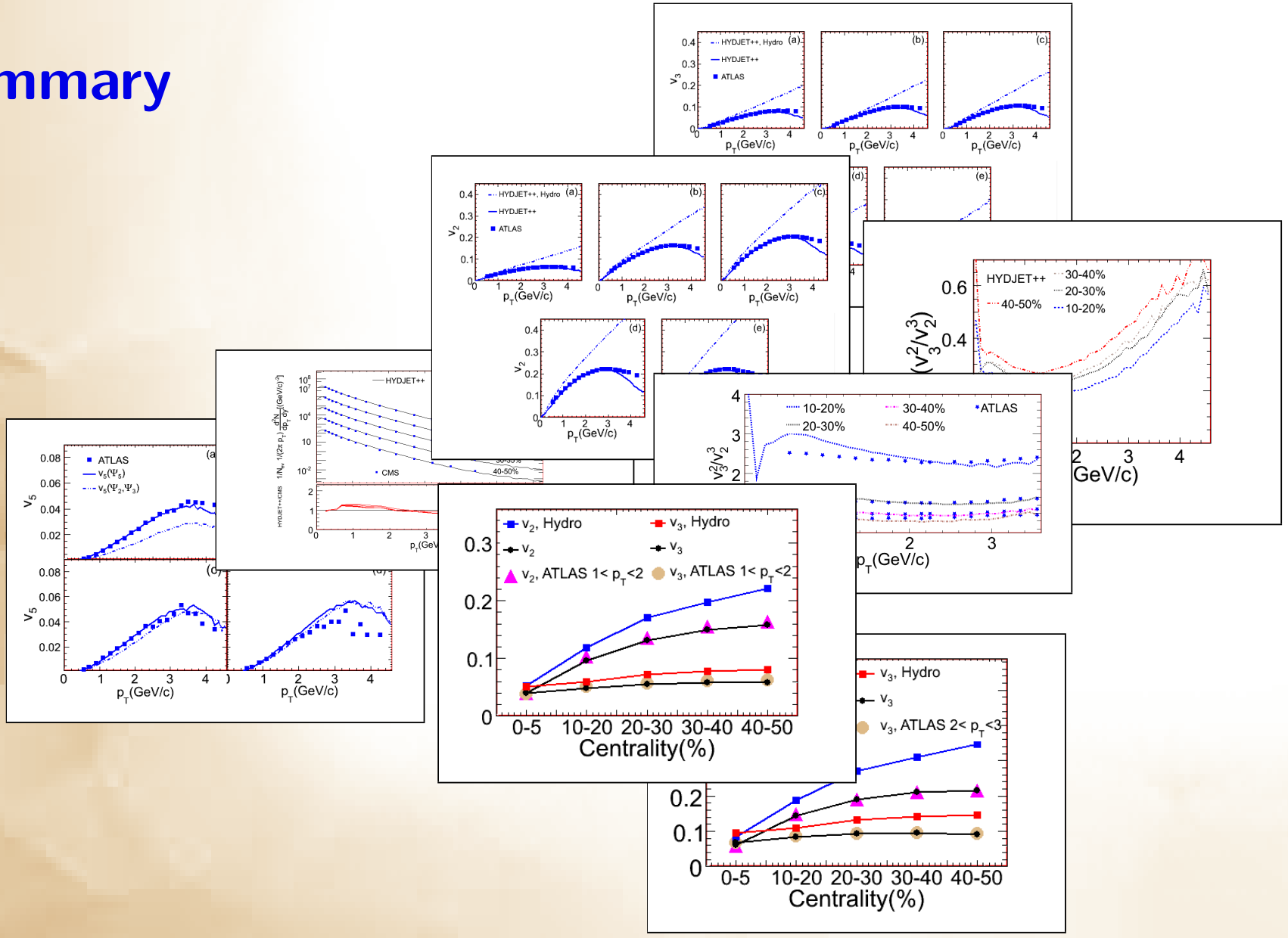
HYDJET++, Hydro
HYDJET++
ATLAS
v_3
v_2
p_T(GeV/c)
(a)
(b)
(c)
(d)
(e)
HYDJET++
30-40%
20-30%
40-50%
10-20%
(v_3^2/v_2^3)
v_3^2/v_2^3
v_5
$v_5(\Psi_5)$
$v_5(\Psi_2,\Psi_3)$
CMS
v_2, Hydro
v_3, Hydro
v_2
v_3
v_2, ATLAS 1< p_T <2
v_3, ATLAS 1< p_T <2
v_3, ATLAS 2< p_T <3
0-5 10-20 20-30 30-40 40-50
Centrality(%)